Investigation of dielectric and electric modulus properties of Al/p-Si structures with pure, 3%, and 5% (graphene:PVA) by impedance spectroscopy

Merve Yürekli[1], Ahmet Faruk Özdemir[1,*] , and Şemsettin Altındal[2]

[1] *Department of Physics, Faculty of Engineering and Natural Sciences, Süleyman Demirel University, Isparta, Turkey*
[2] *Department of Physics, Faculty of Science, Gazi University, Ankara, Turkey*

ABSTRACT

The Z–V measurements were performed in wide-range voltage (± 6 V), and then the real/imaginary parts of ε^* (ε', ε''), M^* (M', M''), Z^* (Z', Z''), tanδ, and σ_{ac} values of the Al/p-Si structure with pure polyvinyl alcohol (PVA) (D1), 3% (D2), and 5% (D3) graphene-doped PVA interfacial-layer were calculated at four frequencies (1, 10, 100, and 1000 kHz). When the frequency in D2 and D3 structures was increased from 1 kHz to 1 MHz, the dielectric constant value changed from 32.47 to 5.12 and from 26.26 to 1.00, respectively. They have a strong frequency dependence due to the presence of interface traps (N_{it}), polarization types, and organic interlayers at low frequencies. The observed anomalous peak in the ε' and ε'' versus voltage curves in the depletion zone is the result of re-structure/re-ordering molecules in these traps under voltage/electric-field, and N_{it} measured frequency ($f = 1/T$). As a result, the ε' and ε'' will be given an excess value to their real-value at lower frequencies. Because N_{it} and dipoles do not have enough time to spin themselves in the direction of the electric field and follow the ac signal at high frequencies, they cannot contribute the true value of them. In general, series resistance (R_s) and the interfacial layer are effective in the accumulation zone, while N_{it} is effective in the depletion region. These findings demonstrate that pure and (Gr:PVA) polymer-films at the M/S interface can be employed successfully in place of standard oxide materials. According to the comparison of dielectric constants, electrical modulus, impedance, and ac conductivity of all three structures at 100 kHz and 1 MHz frequencies, 3% Gr doping to PVA increases interfacial characteristics.

Address correspondence to E-mail: farukozdemir@sdu.edu.tr

Springer

1 Introduction

In general, the fundamental technological and scientific challenge in producing metal interlayer-semiconductor (MIS) type electronic devices is to reduce leakage current Nit, Rs while still providing a high charging or energy storage capacity. Instead of standard developed oxide materials like SiO2 and SnO2, various high-value dielectric interlayers are used at the interface for this purpose. The goal is to improve device performance while decreasing expenses [1–4]. . The conduction/transport-mechanisms (CMs) are influenced by factors such as the grown processes, the function of BH and an interlayer at the metal-semiconductor interface, their homogeneities, Nit (located at the semiconductor/interlayer interface), Rs, doping-level of donor/acceptor atoms, frequency, electric field or voltage ($E = V/d$), and so on [5–10]. At low/intermediate frequencies and voltages, contributions from two or more variables may predominate [11–15]. The employment of such interlayers at the M/S interface, N_{it}, barrier homogeneity, and R_s results in a significant deviation from the ideal scenario [1–7].

Interlayer between M and S enhances capacitor characteristics as well. As a result, it has higher energy storage and easier polarization qualities when subjected to an external force. To increase the quality of these structures, polymer-interlayer and composites have lately been utilized instead of oxides. Because of their large surface area/volume ratio, low cost/weight, mechanical strength, and energy storage qualities. They can also be obtained using simple processes like as sol–gel, electrospinning, and solid–liquid phase separation [16–20]. .

However, using a high-dielectric metal doped polymer as an interlayer may also limit diffusion and reaction at the M/S interface, deactivating many (N_{it}), and therefore improving the electric/dielectric properties of MIS type structures. The presence of N_{it} is typically caused by an interruption of the periodic-lattice structure on the surface of the semiconductor, surface/cleaning processes of the semiconductor, some formed contaminations on the surface of the semiconductor during surface preparations in the laboratory environment, and unsaturated many dangling bounds [1–3]. As a result, frequency dependent electric/dielectric qualities are related to the characteristic N_{it} relaxation-time or angular-frequency ($\omega = 2\pi f = 2\pi/T$). Electrons can become trapped in these N_{it} and behave as positive/negative charges at the interface [1, 2, 16, 21]. Frequency and electric field have a significant impact on electric/dielectric characteristics, electric modulus, and conductivity. As the frequency rises, so do the polarization and N_{it} effects. In other words, when frequency increases, the values of C and G, as well as ε' and ε'' decrease.

The PVA utilized in this work is semi-crystalline, easily soluble in alcohol and water, non-toxic, has better dielectric strength and energy storage capacity values, and is easy to establish hydrogen bonds [22–24]. A single layer of carbon atoms with a 2D hexagonal shape is used to dope graphene into PVA. Because of their great mechanical flexibility, high thermal conductivity, high carrier mobility, and high specific surface area, graphene or graphene-oxide (GO) based polymer-nanocomposites play an important role in semiconductor technology [25–28]. It is also more vital to determine the ideal one rate of doping level into polymers in order to improve the dielectric/electric properties of MPS type structures. Although SiO$_2$ is stable and has a long life, it cannot prevent leakage currents or deactivate/passivate unsaturated chemical bonds. When compared to typical MS and MIS type structures with an insulator/oxide layer developed traditional methods, MPS have become very popular because to their low cost/weight, high surface area, high mechanical strength, flexibility, charge storage capacity, and easy grown methods [19–24]. Furthermore, the use of metal or metal-oxide doped high dielectric polymer interlayers might obstruct the reaction between metal and semiconductor, deactivating numerous undesirable interface traps (N_{it}), and so improving MS structure performance.

In light of the foregoing considerations, we set out to study ε^* ($= \varepsilon' - j\varepsilon''$), M^* ($= M' + jM''$), σ_{ac}, and Z^* ($= Z' + jZ''$) of the D1, D2, and D3 samples at four distinct frequencies (1,10,100, and 1000 kHz). Both C/V and $(G/)/V$ measurements were performed at room temperature in a wide voltage range of ± 6 V. The best one rate of graphene into PVA is %3, and all parameters were found to be a function of frequency in the depletion and accumulation zones due to the impacts of Nit and R$_s$, respectively. In other words, while Nit and polarization are more effective in the depletion zone, Rs and organic layer are more effective in the accumulation zone.

2 Experimental procedures

In this study, Al/p-Si structures containing pure, 3 and 5% Gr:PVA inter-layer were fabricated performed.

Onto same B-doped (p-Si) wafer with the 300 μm, <100> orientation, 2"(= 5.08 cm) diameter, and 0.1Ω.cm resistivity and named the structures as D1, D2 and D3 structures, respectively. Firstly, wafer was cleaned by standard RCA method in ultrasonic bath and dried with N_2 gas. Secondly, 99.999% pure-Au with 150nm was evaporated onto backside wafer at 1μm Torr and was annealed at 500 °C during 5 minutes. Thirdly, polyvinylalcohol (PVA-Mw 130.000 g/mol) was purchased from "Sigma-Aldrich" and Gr-powder was purchased from "Graphene-Chemical Industries", deionize-water and acetic acid (100%, Merck) was used as a solvent and then the prepared (Gr:PVA) solutions were deposited onto front-side Si wafer by utilizing electrospinning method. Thickness of interlayer was estimated as 40nm utilizing Veeco-Dektak 6 M thickness-profilemeter. Finally, 99.999% pure-Al dots with 0.0785 cm^2 and 150 nm thickness was grown onto (Gr:PVA) interlayers. More information on the fabrication-processes and measurement-system can be found in our previous-study [29]. The interlayer thickness (d_i) was found from the interfacial layer capacitance ($C_i = \varepsilon_o A/d_i$) as 40 nm at 1 MHz. After the fabrication processes, the C–V and G/ω–V measurements were performed between 1 kHz-1 MHz at ±6V by utilizing HP 4192 A LF impedance-analyzer and ac/dc converter card to get detail information on the determine frequency/voltage dependent dielectric properties and conductivity of the MPS structure.

3 Results and discussion

Dielectrics utilized at the interface are crucial in electronic device applications such as capacitors, varistors, and transistors because they are a strong indicator of material structure and electrical states. As a result, in addition to the electrical properties, the impact of the frequency of the alternating current electric field supplied to such a structure on the dielectric properties should be investigated. The complex dielectric constant ε^*, loss tangent tanδ, ac conductivity σ_{ac}, and complex M^* and impedance Z^* of Al/p-Si MIS structures produced using PVA interface with and without graphene doping at different rates were investigated in this study using impedance measurements at specific frequencies at room temperature. C/V and G/V measurements were made at 1, 10, 100, and 1000 kHz for all structures (Al/PVA/pSi, Al/%3Gr:PVA/pSi, and Al/%5Gr:PVA/pSi) for this purpose. These C/V and G/V data were used to compute dielectric properties such as ε', ε'', M', M'', σ_{ac}, tanδ, Z' and Z'' as a function of voltage and frequency. The complex dielectric constant (ε^*), which represents the material's interaction in the presence of an applied electric field, is written as: [30–32]:

$$\varepsilon* = \varepsilon' - i\varepsilon'', \tag{1}$$

where the dielectric constant ε' and dielectric loss ε'' are calculated from admittance measurements using the equations:

$$\varepsilon' = \frac{C_m}{C_0} = \frac{C_m d}{\varepsilon_0 A} \tag{2}$$

$$\varepsilon'' = \frac{G_m}{C_0} = \frac{G_m d}{\omega \varepsilon_0 A} \tag{3}$$

C_m and G_m are the measured experimental values, C_o is the capacitance of the empty space, ε_o is the electrical permittivity of the empty space, $\omega(= 2\pi f)$ is the angular frequency, A is the rectifier contact area, and d is the thickness of the organic interlayer. Using ε' and ε'', the dielectric loss tangent may be calculated as follows:

$$\tan\delta = \frac{\varepsilon'}{\varepsilon''} \tag{4}$$

The AC conductivity (σ_{ac}) was derived from the ε'' using the relationship: [4, 6, 32]:

$$\sigma_{ac} = \omega C \tan\delta (d/A) = \varepsilon'' \varepsilon_0 \tag{5}$$

M^*, which is the inverse of ε^* ($M^* = 1/\varepsilon^*$), was calculated by using the ε' and ε'' values to discover the effect of the dielectric material on the relaxation mechanism, as shown below [10, 32–34].:

$$M*(\omega) = \frac{1}{\varepsilon*(\omega)} = M'(\omega) + jM''(\omega) = \frac{\varepsilon'}{(\varepsilon'^2 + \varepsilon''^2)} + j\frac{\varepsilon''}{(\varepsilon'^2 + \varepsilon''^2)} \tag{6}$$

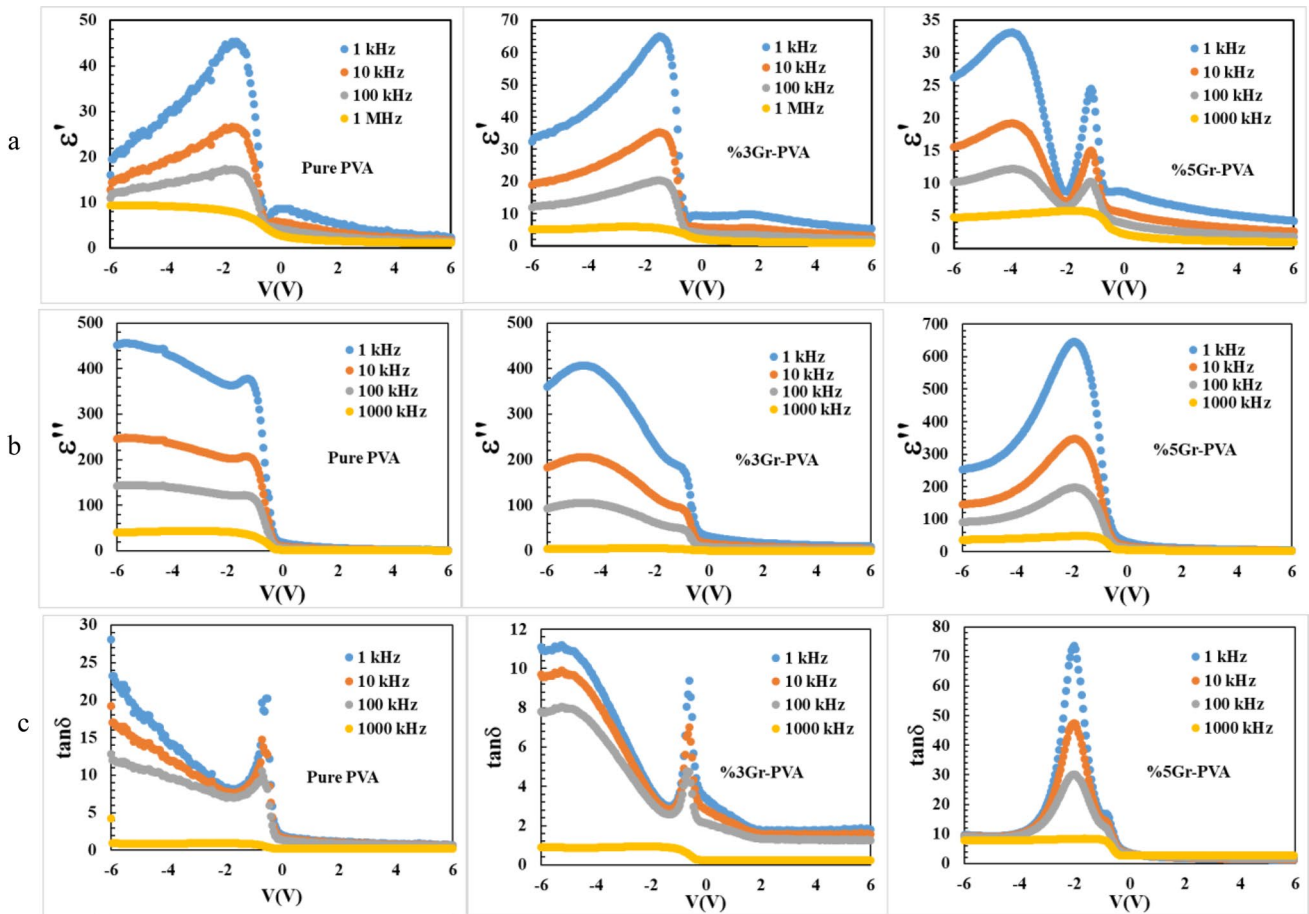**Fig. 1** **a** ε' **b** ε'' **c** tanδ vs. V plots of D1, D2 and D3 structures for different frequencies

The following equation gives Z^* [32, 35, 36];

ε' and ε'' that it is heavily dependent on frequency,

$$Z*(\omega) = \frac{1}{i\omega C_0 \varepsilon *} = Z'(\omega) + jZ''(\omega) = \frac{\varepsilon'}{C_0(\omega\varepsilon'^2 + \varepsilon''^2)} - j\frac{\varepsilon'}{C_0(\omega\varepsilon'^2 + \varepsilon''^2)} \tag{7}$$

Capacitances and conductance were studied for different frequencies between ± 6V voltage range for D1, D2 and D3 structures fabricated using pure PVA, 3% and 5% graphene doped PVA (Gr-PVA) at the Al/p-Si interface. The values of ε', ε'' and tanδ were calculated using Eqs. (2), (3), and (4), and their voltage dependent changes are shown in Fig. 1a–c, respectively. Furthermore, plots of ε' and ε'' for D1, D2, and D3 structures at 100 kHz and 1 MHz are shown in Fig. 2a, b. Figure 1a, b indicate that for three structures, the ε' and ε'' values decrease with increasing frequency in the accumulation and depletion regions, but this decline disappears in the inversion area. We may extrapolate from the behavior of

doping rate, and electric field. The values of ε' and ε'' in the graphs displayed in Fig. 1a, b give the correct value based on the excess ε' and ε'', because charges situated at traps can follow the applied ac signal for low frequency, which depends on their lifetime [32–37]. This contribution to the dielectric properties can be insignificant at high frequencies. Because there are no interface-traps in the inversion zone, the values ε' and ε'' become nearly constant. The voltage dependent profiles of these three structures have also been extracted from the high (0.5 MHz)-low(1 kHz) frequency (C_{HF}–C_{LF}) capacitance method in reference [29], Fig. 6, and they show that the D3 (%5Gr:PVA) structure has fewer interface traps than the others, but interface traps
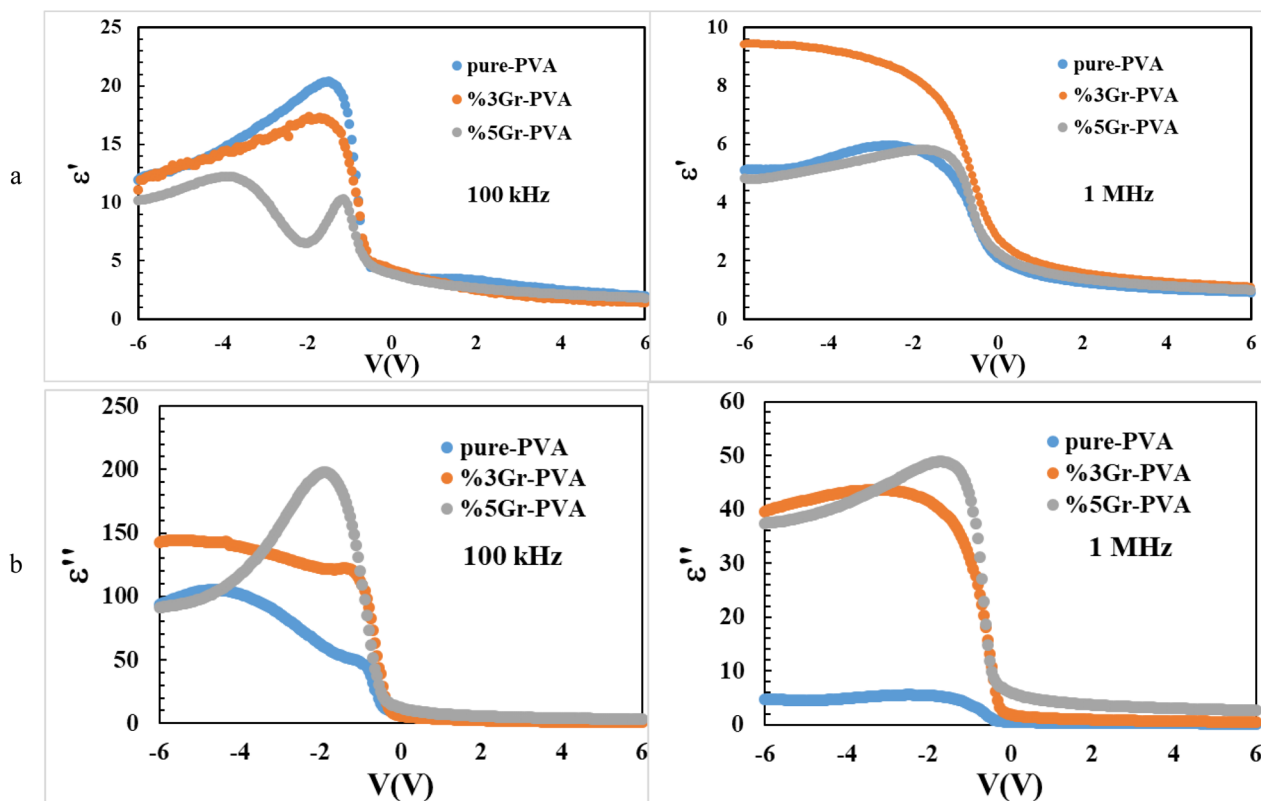
Fig. 2 **a** ε' **b** ε'' vs. V plots for 100 kHz and 1 MHz of D1, D2 and D3 structures

are positioned in two different locations. Furthermore, the interfacial traps in D2 with %3Gr doping are lower than in D1 (pure PVA). As a result, the D2 structure is the best in terms of low interface traps and high dielectric constant, but these values might alter at different voltages due to a unique density distribution of interface states and the polarization effect.

In D1, D2, and D3 structures, anomalous peaks around − 1 V are detected at each frequency, and the amplitudes of these peaks decrease with increasing frequency. Simultaneously, as the doping ratio increases in all three structures, the maximum peak values at the same frequency values fall. These peaks shift towards the origin, that is, towards the positive voltage area, as the doping rate and frequency rise. In contrast to the D1 and D2 structures, the D3 structure has a second peak at − 4 V at the accumulation zone due to the existence of interface-traps placed between the semiconductor and the interface layer in the semiconductor forbidden region at two different sites [19, 20, 30, 31]. Because interface traps are effective at low frequencies and series resistance is effective at high

frequencies, the second peak seen at low frequencies in the D3 structure has turned into a concave curve in 1 MHz frequency, as in the others, indicating that the contribution of active interface traps and bulk traps to the is lost during charge storage and release. Since ε' values of the structures improve the passivation effect at the Gr-doped PVA interface, they are lower than the values of the pure PVA structure, so the amplitude of the peaks is also lower. With an increase in doping % and an increase in frequencies, an extra contribution to polarization occurs, resulting in a ε' fall in D3 values. Surface and interface/dipole polarization can explain this connection [32–40]. . This is also the explanation for the decrease in ε' as the bias voltage is increased.

In terms of ε'' values, the observed low-frequency peaks corresponding to − 1 and − 4 V in D1 and D2 structures, and − 1 V in D3 structures, vanished at high frequencies. Furthermore, as shown in Fig. 2a, b, comparing ε' and ε'' values at 100 kHz and 1 MHz, particularly in the D2 structure, reveals curving concave structure in the depletion zone, whereas peaks in the D3 structure have begun to emerge. This is because the D2 structure reduces the active N_{it}, R_s, and
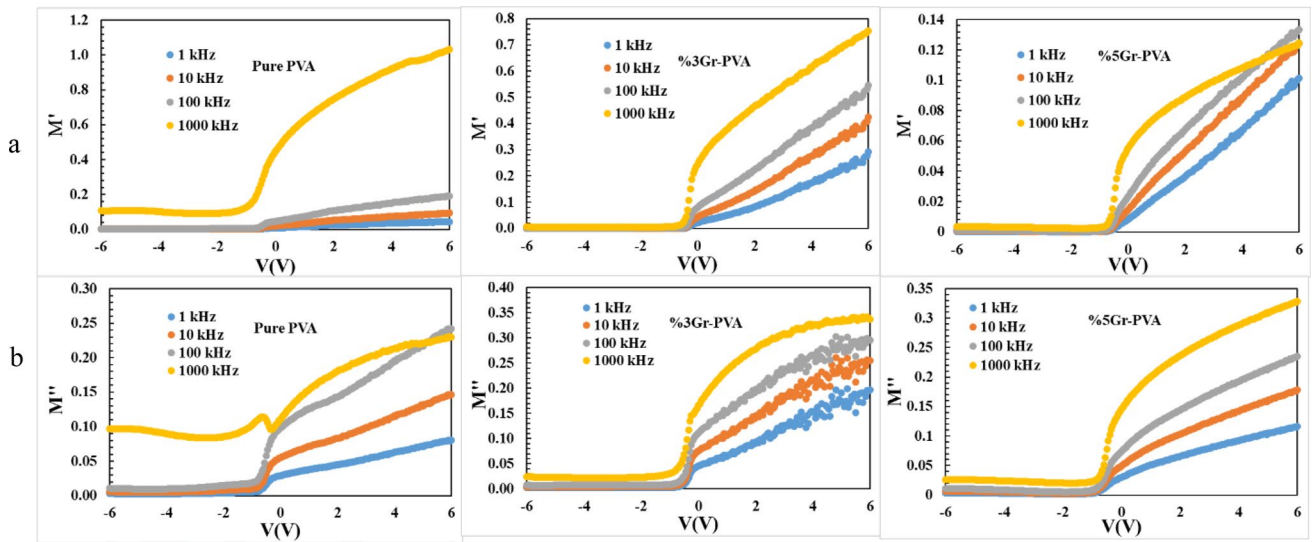
Fig. 3 **a** M' **b** M'' vs. V plots of D1, D2 and D3 structures for different frequencies

polarization in this region. These values also peak at the accumulation region and remain nearly constant. This is due to the decrease in active series resistance in the depletion zone as well as the uniformity of the interfacial layer. Another cause is the dipoles' inertia against the applied electric field, which occurs at both frequencies and in both the depletion and accumulation areas.

The observed in the ε'–V and ε''–V plots (Figs. 1 and 2) at low and intermediate frequencies can be attributed to the presence of interface traps, a specific distribution of them at junctions located in the semiconductor's forbidden bandgap, interface, and dipole polarization. Because the charges at traps can easily follow the ac signal and thus supplied an excess C and G (or ε' and ε'') to the real value of them at lower frequencies due to the low-intermediate frequencies, the period ($T = 1/2f$) is significantly higher than the lifetimes of these traps at low-intermediate frequencies, but at high frequencies becomes lower than of them and thus cannot contribute. The shift peak position, on the other hand, is the outcome of reorganization and reordering of them in the presence of an external electric field.

The values of tanδ for D1, D2, and D3 structures decrease with increasing frequency, as seen in Fig. 1c. In the accumulation and depletion regions of D1 and D2 structures, there is a drop, but it remains constant in the inversion region. Peaks in tanδ values were seen at low frequencies, at − 1 V in the interface structures

of D1, D2, and D3, and at − 2 V in the D3 structure. These peaks vanished at high frequencies. At low frequencies, electrons are orientated prior to the peak and relax after it. Because the peak amplitude falls as frequency increases, the polarization process takes longer and the relaxation process takes longer. The reorganization/restructuring of the charges in the traps under the electric field occurs at the peaks and alters its position in the ε', ε'' and tan δ graphs [37–41].

Furthermore, the decrease in peak behavior produced by the frequency shift in ε', ε'' and tan δ values after the transition from the depletion zone to the accumulation zone is ascribed to the effectiveness of various polarization processes such as space-charge and Maxwell–Wagner [3, 38, 39]. Because polarization processes are triggered by a change in an alternating field generated by the applied electric field and frequency. These systems, which work well at low frequencies, lose potency at high frequencies. In conclusion, the appearance of these peaks is due to N_{it}, R_s, and polarization mechanisms, whereas the shift of the peaks is due to the unique intensity distribution of N_{it} and their life duration (τ).

The values M' and M'' were calculated using Eq. (6), and their voltage dependent changes are shown in Fig. 3a, b. Figure 4a, b shows the plotted M' and M'' values for D1, D2, and D3 structures at 100 kHz and 1 MHz frequencies. M' and M'' grow with increasing frequency in the inversion and depletion zones for D1, D2, and D3 structures, as illustrated
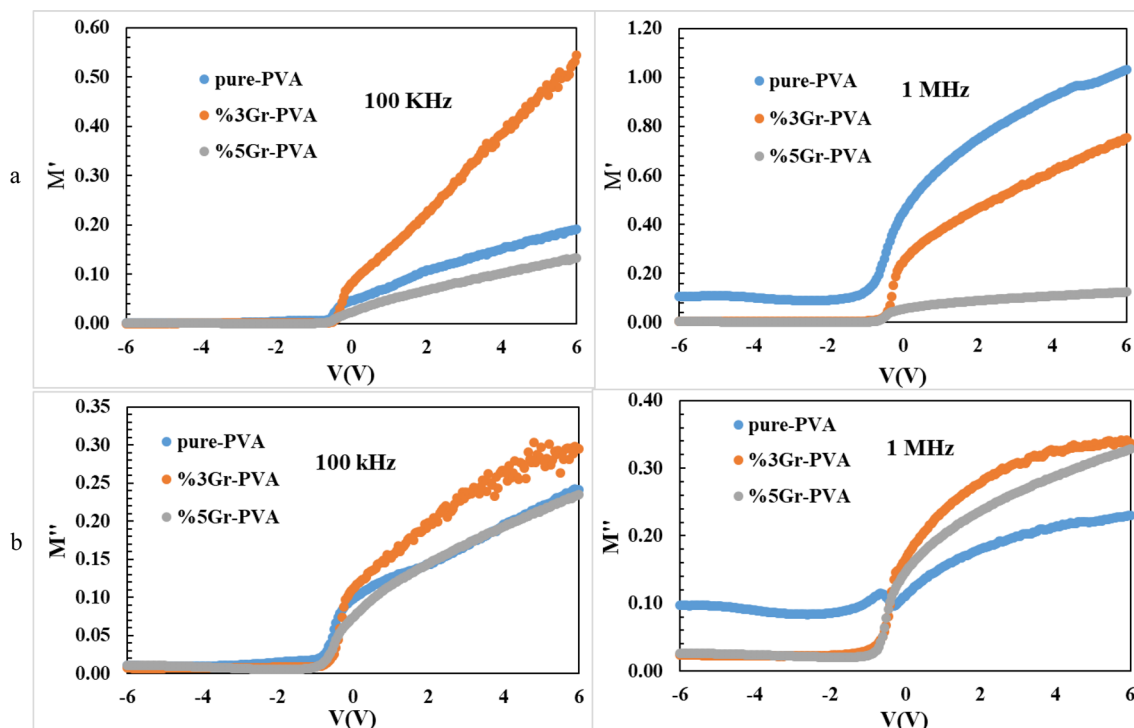
Fig. 4 **a** M' **b** M'' vs. V plots for 100 kHz and 1 MHz of D1, D2 and D3 structures

in Fig. 3a, b, while they are constant or almost nil in the accumulation region. Furthermore, due to the relaxation process, M' and M'' values reach their maximum at high frequencies. As a result, the dielectric polarization mechanism is frequency sensitive. M' and M'' exhibit this behavior due to the relaxation process in the (Gr-PVA) polymer layer and charges in the interface/surface traps [30–33]. Furthermore, M' and M'' values are large because their contribution to the transmission mechanism will grow due to the charge carriers' short distance mobility at high frequency.

Figure 4 shows that, while the M' and M'' values of the D2 and D3 structures at 1 MHz are nearly equal to

zero in the accumulation zone, the M' and M'' values of the D1 structure are constant. This is owing to the reduction in series resistance caused by the addition of Gr to PVA. Furthermore, at 100 kHz and 1 MHz, the M' and M'' values of the D2 structure are greater than those of the D1 and D3 structures

The ac-conductivity (σ_{ac}) values were calculated using Eq. (5), and their voltage dependent changes are shown in Fig. 5. Figure 6 show the plotted σ_{ac} values for D1, D2, and D3 structures at 100 kHz and 1 MHz frequencies. Figure 7 shows that σ_{ac} values are lower in the case of pure PVA interfacial structures than in the case of Gr:PVA structures. Furthermore, as seen in the picture, Gr doping to PVA
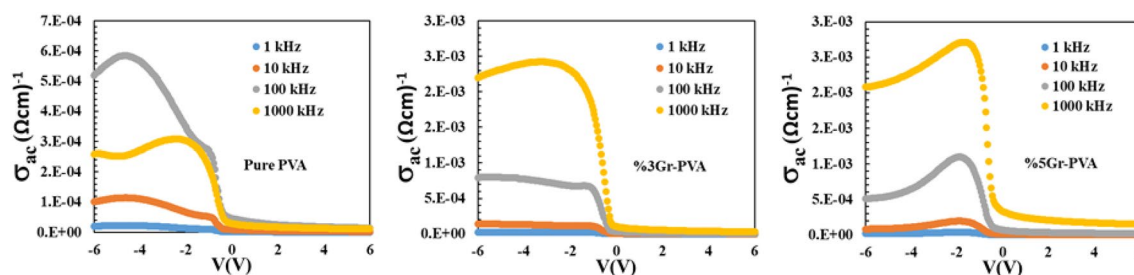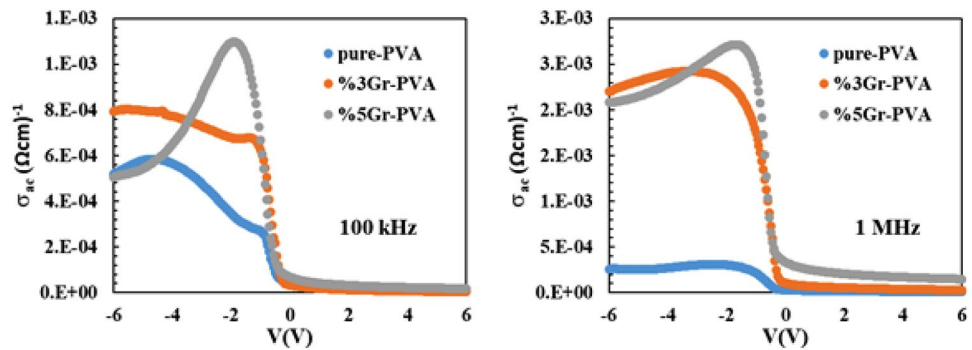

Fig. 5 σ_{ac} vs. V plots of D1, D2 and D3 structures for different frequencies

Fig. 6 σ_α vs V plots for 100 kHz and 1 MHz of D1, D2 and D3 structures

improved conductivity in the depletion and accumulation zones as frequency rose. In the inversion zone, σ_{ac} values are independent of frequency and electric field and decrease to zero, increase abruptly in the depletion region, and remain constant in the accumulation region. At low frequencies, σ_{ac} values are almost frequency independent, therefore conductivity corresponds to dc conductivity. The conductivity increases as the frequency increases due to an increase in the density of mobile ions, and this correlates to the ac conductivity. Furthermore, a rise in σ_{ac} causes an increase in eddy currents, which increases energy/charge loss and $\tan\delta$ [40–48]. Turning to Fig. 6, we can observe that σ_{ac} values in the D2 structure reach a maximum in the accumulation zone at both 100 kHz and 1 MHz, just as the ε'' values in Fig. 2b. Peaks began to appear in the same figure when the Gr doping was 5%. As a result, in the D2 structure, the graphene ratio is the factor that minimizes N_{it}, R_s, and polarization.

Impedance parameters have a significant impact on the electrical transmission mechanism of produced objects. The values of Z' and Z'' were calculated using Eq. (7), and the voltage-dependent changes are shown in Fig. 7. a, b. As shown in Fig. 7a, b, the values of Z' and Z'' decrease with increasing frequency, with their maxima occurring at the lowest value of the considered frequency. At the same time, when the voltage declined, these values decreased and approximated a constant value towards negative voltage levels. This shift in impedance is related to the hoping transport mechanism, which is the transport channel for charge carrier mobility [32, 43]. In recent years, similar results on frequency and doping ratio in MIS and MPS type structures have been reported [49–51].

The phase-angle (θ) relationship between resistance and capacitive currents is as follows [32]:

$$\theta = \tan^{-1}\left(\frac{Z''}{Z'}\right) \quad (8)$$

Thus, the phase-angle (θ) versus voltage curves for D1, D2, and D3 structures were calculated using Eq. (8) at a sufficiently high frequency (1 MHz) and are shown in Fig. 8. As shown in Fig. 8, the value of phase-angle becomes nearly constant in reverse bias voltage for three structures. However, it diminishes with increasing applied bias voltage in the forward bias zone. Furthermore, as the doping ratio Gr into pure PVA increases, the value of phase-angle drops. This demonstrates that the polymer-material has a pure capacitive response and is typically rotated between 0° and 90°.

4 Conclusion

The basic dielectric parameters ε', ε'', $\tan\delta$, M', M'', σ_{ac}, Z', and Z'' of three types of MPS structures (Al/PVA/pSi, Al/%3Gr:PVA/pSi, and Al/%5Gr:PVA/pSi) were examined using $C/G–V$ measurements for various frequencies ranging from ±6V. Because of the existence of Nit and their τ, the ε', ε'' and $\tan\delta$ values were found to decrease with increasing frequency in the depletion and accumulation zones. As a result, it has excessive contributions that represent the genuine dielectric parameter values. Peaks in the depletion and accumulation zones were identified, and these peaks decreased with increasing frequency and graphene doping rates. The increase in ε' and ε'' values with frequency was attributed to doping's extra contribution to polarization. Due to the contribution of charge carriers to the transmission mechanism of short range mobility at high frequencies, the M' and M'' values grow with increasing frequency and reach maximum values in the inversion zone with the relaxation
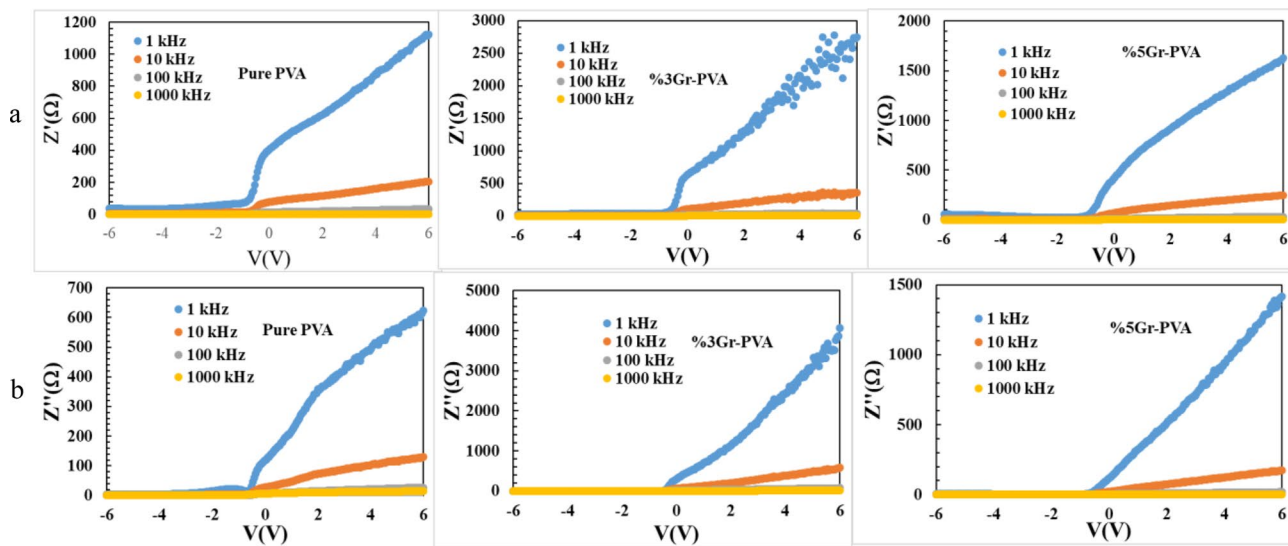
Fig. 7 **a** Z' **b** Z'' vs V plots of D1, D2 and D3 structures for different frequencies
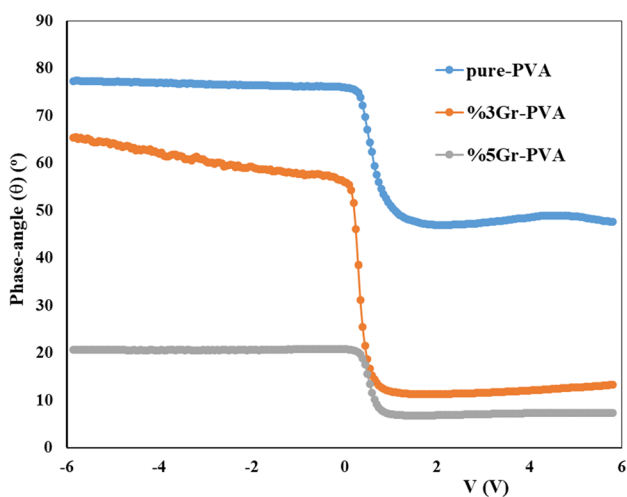

Fig. 8 The variation of phase-angle (θ) with voltage plots of D1, D2, and D3 structures at 1 MHz

process. σ_{ac} values at high frequencies correspond to ac conductivity, while low frequency values belong to dc conductivity. Because of the hope mechanism, the Z' and Z'' values decrease with increasing frequency in the depletion and accumulation zones, and are independent of the electric field and frequency in the accumulation zone. When the ε', ε'', tan δ, M', M'' and σ_{ac} values for D1, D2, and D3 structures are compared at 100 kHz and 1 MHz frequencies. These findings revealed that Gr doped into PVA can cause important changes both in the electrical and dielectric parameters and they can be changed in different voltages especially due to N_{it}, R_s, and polarization. 3% graphene doping rate in PVA revealed better electrical and dielectric parameters. It also demonstrates that, due to their low cost/weight and great flexibility/mechanical qualities, and also can be grown easy technique such as sol-gel, spin-coating, and electrospinning instead of high-cost traditional technique such as thermal oxidation and sputtering.

Author contributions

All authors contributed to the study conception and design. Material preparation, data collection and analysis were performed by MY, AFÖ and ŞA. The first draft of the manuscript was written by AFÖ and all authors commented on previous versions of the manuscript. All authors read and approved the final manuscript.

Funding

Data availability

The datasets generated during and/or analysed during the current study are available from the corresponding author.

Declarations

Conflict of interest The authors have no competing interests to declare that are relevant to the content of this article.

References

1. S.M. Sze, K. Ng Kwok, *Physics of semiconductor devices*, 3rd edn. (John Wiley & Sons, New Jersey, 2007)

2. B.L. Sharma, *Metal-semiconductor Schottky Barrier junctions and their applications* (Plenum Press, New York, 1984)

3. H.C. Card, E.H. Rhoderick, J. Phys. D **4**, 1589–1601 (1971)

4. S. Altındal Yerişkin, M. Balbaşı, İ. Orak, J. Mater. Sci. : Mater. Electron. **28**, 14040–14048 (2017)

5. V.R. Reddy, Vacuum. **164**, 233–241 (2019)

6. A. Buyukbas-Ulusan, S. Altındal-Yerişkin, A. Tataroğlu, J. Mater. Sci. : Mater. Electron. **29**, 16740–16746 (2018)

7. V. Manjunath, V. Rajagopal Reddy, P.R. Sekhar Reddy, V. Janardhanam, C.-J. Choi, Curr. Appl. Phys. **17**, 980–988 (2017)

8. E.A. Akhlaghi, Y. Badali, Ş. Altındal, Y. Azizian-Kalandaragh, Phys. B-Condensed Matter. **546**, 93–98 (2018)

9. V. Rajagopal Reddy, V. Manjunath, V. Janardhanam, Y.-H. Kıl, C.-J. Cho, J. Electron. Mater. **43**, 3499–3907 (2014)

10. S. Altindal, Yerişkin, J. Mater. Sci. Mater. Electron. **30**, 17032–17039 (2019)

11. Ş. Altındal, Ö. Sevgili, Y. Azizian-Kalandaragh, J. Mater. Sci.: Mater. Electron. **30**, 9273–9280 (2019)

12. J.H. Werner, H.H. Güttler., J. Appl. Phys. **69**, 1522–1533 (1991)

13. Y.P. Song, R.L. Van Meirhaeghe, W.H. Laflère, F. Cardon, Solid State Electron. **29**, 633–638 (1986)

14. A. Büyükbaş Uluşan, A. Tataroğlu, Y. Azizian-Kalandaragh, Ş. Altındal, J. Mater. Sci. **29**,, 159–170 (2018)

15. R.T. Tung, Appl. Phys. Rev. **1**, 011304 (2014)

16. M. Sharma, S.K. Tripathi, Appl. Phys. A **113**, 491 (2013)

17. A. Wankei Wan, L. Dawn Bannerman, Yang, H. Ma, Polym Cryog. Adv. Polym. Sci. **263**, 7–8 (2014)

18. V.R. Reddy, Thin Solid Films. **556**, 300 (2014)

19. O. Çiçek, H.U. Tecimer, S.O. Tan, H. Tecimer, I. Orak, Ş. Altindal, Compos. Part. B **113**, 14–23 (2017)

20. E. Marıl, S. Orkun Tan, Ş. Altındal, İ. Uslu, IEEE Trans. Electron. Dev. **65**, 3901–3908 (2018)

21. E.H. Nicollian, A. Goetzberger, Bell Syst, Tech. J. **46**, 1055–1133 (1967)

22. A. Tataroglu, Ş Altındal, Y. Azizian-Kalandaragh, Phys. B **582**, 411996 (2020)

23. H.S. Nalwa, *Handbook of low and high dielectric constant materials and their applications* (Academic Press, London, 1999)

24. K.C. Kao, *Dielectric phenomena in solids* (Elsevier, London, 2004)

25. K.K. Sadasivuni, D. Ponnamma, J. Kim, S. Thomas, *Graphene-based polymer nanocomposites in electronics* (Springer, Switzerland, 2015)

26. S.K. Shahenoor Basha, K. Vijay Kumar, G. Sunita Sundari, M.C. Rao, Adv. Mater. Sci. Eng. (2018). https://doi.org/10.1155/2018/4372365

27. A. Kaya, S. Alialy, S. Demirezen, M. Balbaşı, S.A. Yerişkin, A. Aytimur, Ceram. Int. **42**, 3322–3329 (2016)

28. S. Mansouri, B. Coskun, L. El Mir, A.G. Al-Sehemi, A. Al-Ghamdi, F. Yakuphanoglu, J. Electron. Mater. **47**, 2461–2467 (2018)

29. S. Altındal, Y. Şafak Asar, J. Mater. Sci: Mater. Electron. **32**, 22860–22867 (2021)

30. S. Kasap, P. Capper, *Springer handbook of electronic and photonic materials* (Springer, New York, 2006)

31. G.G. Raju, *Dielectrics in electric fields*, 2nd edn. (CRC Press, Boca Raton, 2017)

32. A.M. Akbas¸, A. Tataroğlu, Ş. Altındal, Y. Azizian-Kaland-aragh, J. Mater. Sci: Mater. Electron. **32**, 7657–7670 (2021)

33. S. Ishaq, F. Kanwal, S. Atiq, M. Moussa, U. Azhar, I. Gul, D. Losic, Results Phys. **11**, 540–548 (2018)

34. H.A. Chaube, V.A. Rana, Solid State Phenom. **209**, 182–185 (2014)

35. G.E. El-Falaky, O.W. Guirguis, A.B.D. El-Aal, Prog Nat. Sci. : Mater. Int. **22**, 86–93 (2012)

36. A. Mars, H. Essaidi, J. Ouerfelli, J. Alloys Compd. **688**, 553–564 (2016)

37. C. Bilkan, S. Altındal, Y. Azizian-Kalandaragh, Phys. B **515**, 28–33 (2017)

38. Y. Azizian-Kalandaragh et al., J. Mol. Struct. **10**, 1224 (2021)

39. G.E. Demir, İ. Yücedağ, Ş. Altındal, J. Mater. Sci.: Mater. Electron. **31**, 16324–16331 (2020)

40. P.T. Oreshkin, *Physics of semiconductors and dielectrics* (Vysshaya Shkola, Moscow, 1977)

41. G. Ersöz, I.Y.Y. Azizian-Kalandaragh, I. Orak, S. Altındal, IEEE T Electron. Dev. **63**, 2948–2955 (2016)

42. S. Karadas, S. Altındal Yerişkin, M. Balbaş, Y. Azizian-Kalandarag, J. Phys. Chem. Solids. **148**, 109740 (2021)

43. İ. Orak, A. Karabulut, Turkish J. Phys. **44**, 1 (2020)

44. S.O. Tan, O. Çiçek, Ç. Gökhan Türk, Ş. Altındal, Eng. Sci. Technol. **27**, 101017 (2022)

45. H. Uslu, ¸S, T. Altındal, I. Tunç, T.S. Uslu, Mammadov, J. Appl. Polym. Sci. **120**, 322–328 (2011)

46. A. Karabulut, A. Türüt, Ş Karataş, J. Mol. Struct. **1157**, 513–518 (2018)

47. A. Kyritsis, P. Pissis, J. Grammmatikakis, J. Polym. Sci. Pol. Phys. **33**, 1737–1750 (1995)

48. Z. Tekeli, M. Gökçen, S. Altındal, S. Özçelik, E. Özbay, Microelectron. Reliab. **51**, 581–586 (2011)

49. S. Altındal Yerişkin, E. Eebilen, M. Tanrıkulu, Ulusoy, Mater. Chem. Phys. **303**, 127788 (2023)

50. S. Demirezen, S. Altındal Yerişkin, J. Mater. Sci: Mater. Electron. **32**, 25339–25349 (2021)

51. Z. Berktaş, E. Orhan, M. Ulusoy, M. Yildiz, Ş. Altındal, Appl. Electron. Mater. **5**, 1804–1811 (2023)